

A novel experimental approach to uncover the nature of cosmic-ray Deuterium

F. Dimiccoli^{1,2,*} and F. M. Follega^{1,2,†}

¹*University of Trento, Department of Physics, V. Sommarive 14, I-38123, Trento, Italy*

²*INFN-TIFPA, V. Sommarive 14, I-38123 Povo (Trento), Italy*

(Dated: January 8, 2025)

Studying the isotopic composition of cosmic-rays (CRs) provides crucial insights into the galactic environment and helps improve existing propagation models. Special attention is given to the secondary-to-primary ratios of light isotopic components in CRs, as these measurements can offer complementary data compared to traditional secondary-to-primary ratios like B/C. Recently, a precision measurement of the Deuterium (D) abundance in CR in the 2-21 GV rigidity range provided by the AMS02 experiment unexpectedly detected an excess of D with respect to its expected secondary nature, opening the field for new measurements at high rigidity to determine how the spectrum evolves and whether there is confirmation of a primary or primary plus secondary origin. While there are theoretical models that attempt to explain this excess, the experimental uncertainties on D production cross-sections and on CR propagation models remain significant, and only new and precise measurements can dissipate existing doubts. In this work we review the current experimental scenario and we propose a dedicated experiment able to extend the D abundance measurement up to 100 GeV/nuc without the need of a magnetic spectrometer, using a multiple scattering based technique for the measurement of particle momentum. The expected performances of the proposed detector were assessed through a dedicated simulation using the GEANT4 package, and its role in the current particle physics scenario is discussed.

I. INTRODUCTION

Studying the flux of cosmic-ray Deuterium (D) is pivotal to probe the mechanisms of cosmic-ray propagation and improve the understanding of the underlying astrophysical processes. For long time, Deuterium was believed to be a pure secondary [1], overwhelmingly produced through the spallation of heavier nuclei, mainly ⁴He interacting with the interstellar medium (ISM) [2].

The understanding of the propagation mechanisms of this element is crucial for multiple reasons. First, being D significantly lighter with respect to other secondary elements like B, it can effectively probe CR propagation at larger galactic distances [3] and measurements of the ratio of D against primaries like p and ⁴He, could provide insights into the spallation processes and the composition of the ISM. Second, as it is produced by a light primary like ⁴He, it offers complementary insights compared to heavier secondary-to-primary ratios such as B/C, which have traditionally been used as tools to study CR propagation. Eventual discrepancies in diffusion behaviors at different Z may reinvigorate discussions about scenarios which violate the CR propagation universality postulate [4]. Third, the development of reliable models of CR propagation faces important theoretical challenges, due to the limited experimental knowledge of inelastic cross section for all the involved nuclei [5]. Therefore, a measurement of deuteron flux at high energies could be used to constrain these uncertainties. Moreover, improving the understanding on the propagation process of CR in

the galaxy, and thus of the property of the galactic environment itself, has also profound implications regarding the prediction of the amount of light anti-nuclei (e.g. \bar{p} , \bar{D}) produced by spallation reactions. This estimation is pivotal in the indirect searches for Dark Matter (DM), since the exotic production of light anti-nuclei in the DM annihilation process is one of the most promising channels for its indirect detection. In particular, the production of \bar{D} in CR spallation reaction is kinematically disfavored. As such, theoretical predictions show that the \bar{D} is an almost background-free channel for indirect DM searches [12]. In this context, the study of the Deuterium propagation assumes also the role of a proxy for the behavior of the \bar{D} nuclei in the galaxy.

All the arguments above assume that deuterons predominantly originate as a secondary component. However, the unambiguous identification of deuterons as pure secondary cosmic-rays requires measuring the rigidity dependence of its flux at high energies and in particular the ratio with its supposed progenitor, the D/⁴He ratio. Until recently, this has not been achieved due to the experimental difficulties involved.

Recent measurements from the Alpha Magnetic Spectrometer (AMS02) on the International Space Station have provided detailed spectra of cosmic-ray deuteron up to 21 GV [6]. Surprisingly, the deuteron spectrum at high energies is significantly harder than what is typically expected for secondary species. The rigidity dependence of these particles closely resembles that of protons (p), yet it differs significantly from that of ³He, another isotope produced by ⁴He spallation. This feature confirms the presence of an excess of high energy D with respect to the one expected from secondary production alone, suggesting the existence of a primary-like deuteron component. Given the implications of these new data on

* francesco.dimiccoli@unitn.it

† francesco.follega@unitn.it

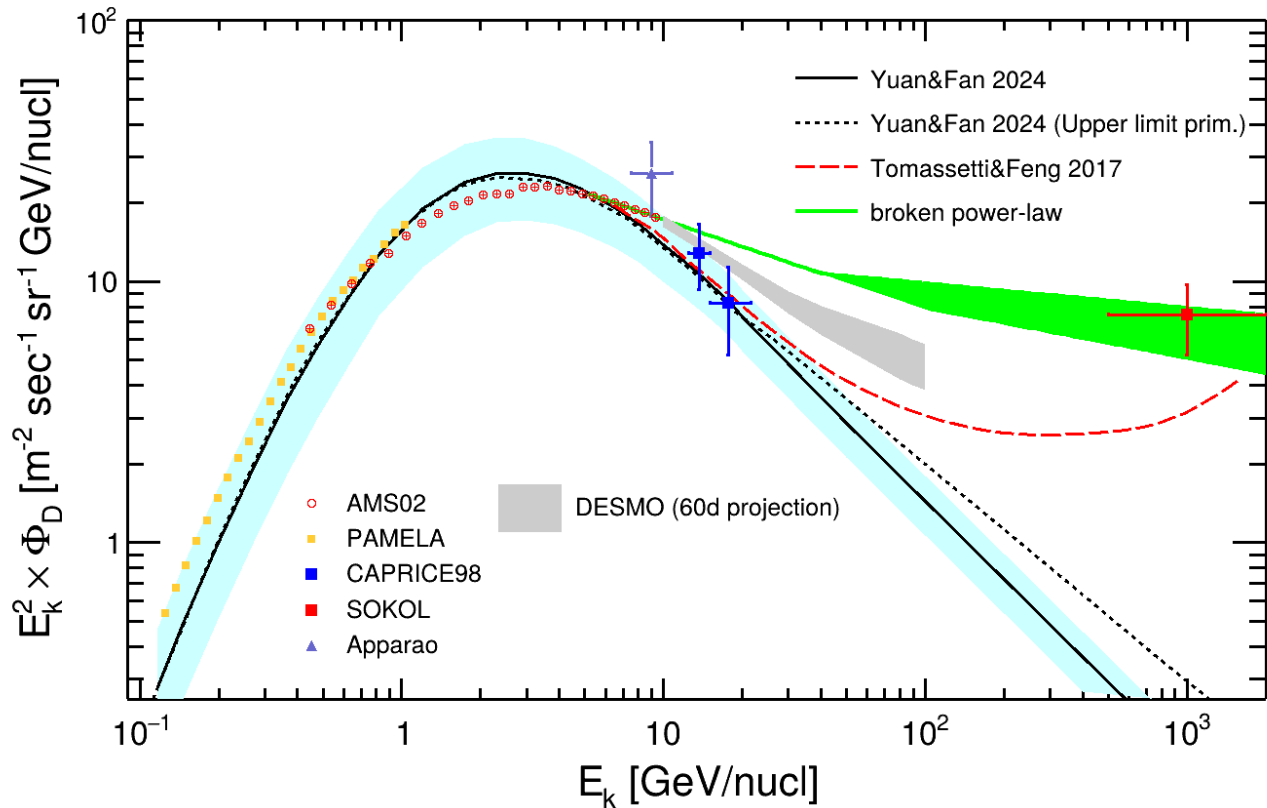


FIG. 1. Measurements and models of Deuterium flux as a function of the kinetic energy per nucleon (E_k), and multiplied by E_k^2 , are shown. Data points represent experimental measurement by AMS02 [6], PAMELA [7], CAPRICE98 [8], SOKOL [9] and Apparao et al. [10]. The black lines represent the models obtained by [11], in the case of purely secondary deuterons (continuous line) and considering the calculated upper limit of primary contribution (dotted). These models were extrapolated at high energies with a single power-law trend above 20 GeV/nucl. The green line + band represents the extrapolation of AMS02 data calculated as described in Section II. The red dashed line shows the model presented in [4]. The gray band represents the projection of an hypothetical measurement by the DESMO detector (Section III) in 60 days, based on the performance estimated in the following section of this work, assuming a deuteron flux dependence $\propto E_k^{-2.7}$ (see Section IV).

the phenomenology of CR propagation, the situation deserves more clarification on the experimental side, possibly extending the charted rigidity range for this measurement.

In this work, we review the current state of the measurements and the models concerning cosmic-ray deuterons, emphasizing on the hints of a primary-like nature. In the second part, we propose DESMO (DEuterio con Scattering MultiplO), a balloon-borne experiment, designed to measure deuteron flux at higher energies.

II. SCRUTINIZING MEASUREMENTS AND MODELS ABOUT HIGH-ENERGY DEUTERON FLUX

The current experimental and theoretical knowledge about high-energy D cosmic-ray flux is summarized in Figure 1. As can be seen, AMS02 is the only high-

precision measurement available at energies that exceed the domain of solar modulation, probing the spectral shape of this nucleus above 1 GeV/nucl. As introduced above, the hardening of the deuteron spectrum toward the higher energies reported by AMS02 was unexpected, because traditional astrophysical models do not predict significant D production outside of the Big Bang nucleosynthesis (BBN) [13]. Recent theoretical studies [11] made use of the numerical code GALPROP [14] to simulate the D galactic diffusion and showed that, considering all the contributions from fragmenting nuclei up to $Z=28$, it is possible to explain the AMS02 measurement within a secondary production framework. The model is with AMS02 results within errors, dominated by the uncertainty on diffusion parameters and on nuclear cross sections. This result underlines the importance of the contribution given by the fragmentation of heavy nuclei to the Deuterium flux. However, considering the scarcity of direct cross-section measurements, this interpretation

of the measured excess of deuterons is currently object of debate across the scientific community [15]. Nevertheless, this study obtains an upper limit for an hypothetical primary component ($D/H \leq 1.6 \times 10^{-3}$) that could explain the AMS02 measured data, that would imply a much higher abundance of Deuterium with respect to the one expected from BBN and/or a much more efficient acceleration mechanism for D. In Figure 1, we reported also these predictions, extrapolated above 20 GeV/nuc, assuming a constant power-law dependence. Currently, other measurements of the deuteron flux at high energies exist, independently conducted over the years by various experimental apparatuses. We firstly report the result of the deuteron flux obtained by Apparao et al. [10] and reported in other works ([9],[4]), which is compatible with the AMS02 measurement. At higher energies, only few experimental points with large uncertainties are available. The measurements provided by CAPRICE98, shown in Figure 1, cover an higher energy range and are in better agreement with the extrapolated model prediction with respect to the trend of the AMS02 data. However, despite the large error bars, they still hints toward an excess of high-energy deuterons. Finally, indications of anomalous D abundance at extremely high-energy were provided by the SOKOL satellite experiment [9]. Discriminating between the different shapes of the hadronic cascades induced by D and p nuclei at very high energies, they were able to measure a fraction of D in cosmic hydrogen of $(37.0 \pm 7.6)\%$ between 1 and 4 TeV of total energy. We converted this measurement in an absolute D flux measurement using as an anchor the integral of the proton flux measured by the DAMPE experiment [16] in the same energy range. The result of this calculation, converted in kinetic energy per nucleon, is also shown in the Figure. Moreover, authors of [4] have shown that such measurement can be explained in terms of standard mechanisms of D production (red long-dashed line in Figure 1) assuming a different acceleration mechanisms for light and heavy primaries. If confirmed, this scenario would have profound implications, since the secondary to primary ratios involving the heavy primaries would not be able to place constraints on the production of light isotopes or anti-particles. On this topic, we propose an extrapolation of the AMS02 data, shown in green in Figure 1, that interestingly enough aligns with the SOKOL measurement. We obtained their spectral index ($\gamma = -2.34 \pm 0.01$) from a single power-law fit above 5 GeV/nuc, and introduced an high-energy spectral index change, $\Delta\gamma$, ranging from 0.15 to 0.20, as observed by AMS02 in primary nuclei [17]. This spectral shape was modeled using a broken power-law with a rigidity break point between 80 and 200 GV. The green band represents the variability of the model under these parameter variation and aligns with the SOKOL observations.

Basing on the current theoretical and experimental knowledge of the topic, we depict three scenarios: a) D is a secondary species or it has a limited primary-

like component, as shown in [11]; b) D is a secondary species, but produced by primaries accelerated with different mechanisms, as hypothesized in [4]; c) D follows a hard primary-like power-law spectral shape that continues the trend measured by AMS02. Only through a precise measurement of the D flux spectral index at higher energies the distinction between these three scenarios is possible.

To address this challenge, we propose a new experimental strategy that builds on recent advancements in detection technology, keeping as a cornerstone stringent constraints on mission complexity and cost. Leveraging on the methodology shown in [18], which utilizes multiple scattering for isotopic identification, we propose DESMO for a two-months balloon flight. DESMO is a new and efficient solution for the study of cosmic-ray isotopes at high energies with a relatively compact and light design, operating in the rigidity range between 20 and 200 GV. With the gray band in Figure 1 we show a projection of a 60 days long DESMO measurement based on the performances estimated in the following sections and its ability to discriminate between the aforementioned (a), (b) and (c) scenarios, finally shading light on the origin of cosmic-ray deuterons.

III. THE DESMO CONCEPT

The concept behind DESMO is to obtain a lightweight, relatively cheap and robust detector able to provide a measurement of the D flux, that can operate as light payload in a long duration balloon flight. To fulfill this vision, we imposed stringent requirements on the total detector mass (below 100 kg), on the total tracking area (below 2 m²) and on the total detector length (below 1.6 m), which makes DESMO at least an order of magnitude smaller than future and current cutting-edge experiments like AMS02.

This can be achieved using a novel technique for isotopic identification in cosmic-rays, based on multiple scattering, which exploits the different angles at which isotopes of the same velocity but different masses are scattered. This approach has already been proposed for measurement of particle momentum [19], and offers an interesting alternative to traditional magnetic spectrometers, which face limitations in resolution and complexity when targeting high energies. As shown in [18], it is possible to exploit the dependence of the multiple scattering effect with the particle momentum to obtain a measurement of the latter without the need for strong magnets to bend particle trajectories. This, in conjunction with a measurement of particle velocity, allows for a mass measurement and thus for an identification of isotopes. DESMO is composed of two fundamental modules: the first measures the velocity of the incoming particle, the second measures the average displacement induced by the multiple scattering on the particle trajectory. Its final design is shown in Figure 2. The first module, a particu-

larly compact design of Ring Imaging Cherenkov detector (RICH), makes use of a spherical mirror and fulfills the first task, besides estimating the incoming particle charge Z . The second module, the Multiple Scattering Isotope Separator (MSIS), is able to separate different masses among nuclei of same Z and velocity, providing also an independent charge measurement.

A. The MSIS detector

The multiple scattering approach involves tracking the deflections of charged particles as they pass through a series of thin targets contained in several measuring stations. Every measuring station consists of two tracking planes and of a high-density and high- Z target, to induce the deviation of the particle trajectory by multiple scattering. We call this fundamental unit of the detector the PPT module (Plane-Plane-Target). Each PPT module measures the incoming particle trajectory and deviates it for the next measurement. The MSIS detector is composed of eight identical PPT modules, and of two additional tracking planes placed at its bottom to measure the deviation induced by the last station and obtain a total of eight measurements. In this way, a tower of N different stations can provide the measurement of N different trajectories and thus $N-1$ scattering angles θ_i . This method has been validated through extensive simulations using the GEANT4 package [20], demonstrating its capability to identify $Z=1$ isotopes at high energies [18]. The angle θ_i is measured using the linear displacement $d_i = S \tan \theta_i \approx S\theta_i$ of the hit measured by the first tracking plane with respect to the linear extrapolation of the trajectory measured by the precedent PPT module, where $S=6$ cm is the spacing between two subsequent PPT modules. The eight displacement measurements are combined to obtain an average displacement d , which is proportional to the multiple scattering angle θ_{MS} :

$$d = \frac{\sum_i d_i}{8} \approx \frac{\sum_i S\theta_i}{8} \approx S\theta_{MS}$$

The silicon planes of each PPT modules are all equal, each measuring 33 cm \times 33 cm and 3 mm thick, with a 6 cm separation between them. Typical values of displacements for (10-100) GeV/nucl p and D in MSIS are respectively in the range between 10 μ m and 200 μ m, so high spatial resolution is critical for accurately determining scattering angles. This can be achieved with a matrix by ALPIDE pixel sensors (28 \times 28 μ m²), which, determining the centroid of the pixel cluster, can reach a sub-pixel spatial resolution of the order of 5-10 μ m [21], with low material budget per tracking plane. Tracking detectors of this kind have already been produced and integrated in space detectors [22, 23]. A target material, with high density and high- Z properties, is essential for inducing significant scattering, which is then measured by the tracking planes. An active material like a crystalline scintillator, such as Bismuth-Germanate (BGO)

with an effective Z of 74 and a density of 7.13 g/cm³ [24], allows for energy deposition measurements and provides a fast signal that can serve as a trigger for DESMO. For these reasons, a 14 mm thick BGO target is positioned next to the second tracking plane of every PPT module. By measuring energy deposition, each target provides an independent measurement of the incoming particle's charge Z . The majority of nuclei in the DESMO target energy range are in the Minimum Ionizing Particle regime and penetrate many of such targets before having a significant chance for inelastic interactions. Thus, the combinations of the energy deposition measurements from the first two BGO targets can be used to obtain a precise charge measurement. From studies performed on the GEANT4 simulation of the MSIS we estimated a charge resolution of $\Delta Z/Z \sim 0.04$, lowering the contamination from $Z \geq 2$ nuclei on the D signal to negligible levels. Additionally, BGO offers the opportunity for an optional target segmentation, enabling a rough trajectory estimate to trigger only nearby silicon pixel modules, significantly reducing their readout power requirements.

The MSIS design specifications were determined through an optimization process detailed in Appendix B, aimed at maximizing the precision of the average displacement d , while adhering to the design requirements outlined in at the beginning of this section. The performance of this design has been validated through simulations, demonstrating its capability to effectively separate protons and deuterons at high energies. More details on this can be found in [18]. The optimization of the PPT module design involved extensive simulations using the GEANT4 package and additional tools reproducing the digital signal of the pixels [25]. These simulations accounted for various factors, including the energy range of interest (10-100 GeV/nucl), the spatial resolution of the silicon planes, and the scattering properties of the target. A detail study is shown in Appendix B. These studies showed that the DESMO detector could achieve a significant separation power (defined as in [26]) for $Z = 1$ isotopes, making it a promising tool for a cosmic-ray D measurement.

B. The RICH detector

Particle kinetic energy per nucleon E_k , measured in GeV/nucl, can be obtained from a measurement of particle velocity ($\beta = v/c$), through the relation

$$E_k = \frac{E_{kin}}{N_{nucl}} = m_{nucl}(\gamma - 1) \quad , \quad m_{nucl} = \frac{N_p m_p + N_n m_n}{N_p + N_n}$$

where N_{nucl} is the number of nucleons, m_{nucl} is the mass of the average nucleon, with N_p (N_n) and m_p (m_n) that are respectively the number and mass of the protons (neutrons). A precise velocity measurement is needed in the 10-100 GeV/nucl energy range. The combined requirements of precision and compactness in the design can be achieved only using a Cherenkov detector [27].

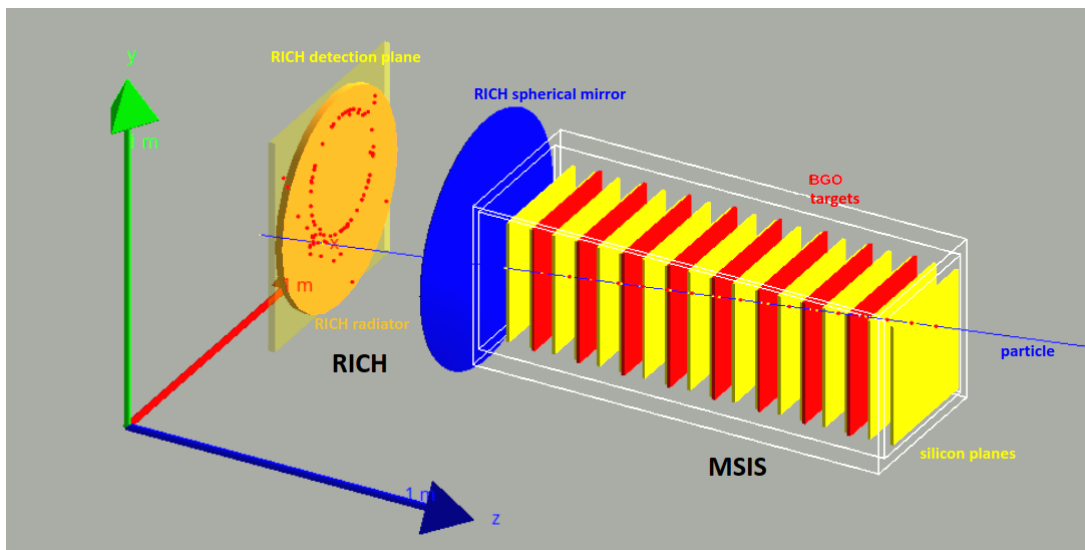


FIG. 2. Rendering 3D of the DESMO detector, with its principal components labeled: RICH and MSIS sub-detectors (see the text). A simulated D event of generated energy 50 GeV/nucleon is also shown. The red points represent the hits of the primary particle and of the Cherenkov photons produced by the particle passage, measured by the detector active areas. The yellow points represent the multiple scattering interactions. In particular, the reflected Cherenkov ring is visible on the RICH detection plane. The tracks of secondary particles were not drawn for visualization purposes. The green, red and blue arrows show a 1 m length in the x , y and z directions as a visual scale reference.

A compact design Ring Imaging Cherenkov (RICH) detector was devised for this purpose, based on a 2 cm thick layer of Silica Aerogel (SiO_2) radiator with spectral index of $n=1.05$ and density of 0.2 g/cm^3 [28–30].

A spherical mirror (1 m radius, 50 cm diameter) re-focuses back Cherenkov photons onto a SiPM detector array (83×83 chips, $6 \times 6 \text{ mm}^2$ each) positioned right below the radiator. Each chip is composed of individual cells with side dimensions ranging from 10 to 100 micrometers. A more detailed discussion of the spatial resolution attainable by this detector plane is reported in Appendix C. Figure 2 shows graphically the proposed design of RICH integrated in the DESMO detector. The detector’s feasibility was initially evaluated for perpendicular tracks [18]. This study extends the evaluation to a realistic cosmic-ray scenario simulating single charged high energy particles with inclinations up to 20° (maximum angular acceptance of the MSIS detector below) and generic impact point, using the GEANT4 simulation toolkit. In the general case, the Cherenkov cones are re-focused by the mirror in an ellipse on the detector plane described by $X^2/S_A^2 + Y^2/S_B^2 = 1$, with

$$\begin{aligned} X &= (x - X_0) \cos \alpha + (y - Y_0) \sin \alpha, \\ Y &= -(x - X_0) \sin \alpha + (y - Y_0) \cos \alpha, \end{aligned}$$

where X_0 , Y_0 parameters are the ellipse center coordinates, the semi-axes S_A , S_B , and the angular tilt α between the ellipse “horizontal” axis and the horizontal direction. This curve is reconstructed by the RICH readout plane. Cherenkov photon hits are fitted to extract ellipse parameters (S_A , S_B , X_0 , Y_0 , α). The precision on the pa-

rameters is limited by the total number of photons collected, which is primarily influenced by the amount of radiator traversed by the charged particle and by the quantum efficiency of the SiPM [31]. For the latter we assumed a conservative constant value of 30% (see Appendix C). Moreover, the occurrence of large scattering phenomena like the Rayleigh scattering or auto-absorbing effect of the radiator can further limit the amount of useful photons. Such effects are accounted for in the simulation, modeling the optical properties of Silica Aerogel material [32]. Also imperfection of the mirror surface were taken into account, adding a smearing in the reflected photon direction of the order of 0.5 mrad [33]. Hits coming from photons not correctly focused, because of scattering phenomena or mirror imperfections, can be excluded from the analysis with an iterative fit procedure. The procedure can be summarized as follows: a first fit of the ellipse is performed taking into account all the available photon hits, but it is constrained using informations such as the estimated position of the center-of gravity of the hits and the crossing point of the particle with the RICH readout plane, extrapolated from the track measured by MSIS (“Hotspot”). In particular, hits inside 1 mm radius from the Hotspot are not considered. Then, a series of subsequent iterations are performed repeating the fit, but considering only the hits in the vicinity of the previous estimation of the ellipse. This selection is performed by studying the distribution of the distances from the available hits and the fitted ellipse. The standard deviation σ of the resulting histogram is calculated and only hits within 2σ from zero are retained. It is worth noticing that previously discarded hits can be recovered if their

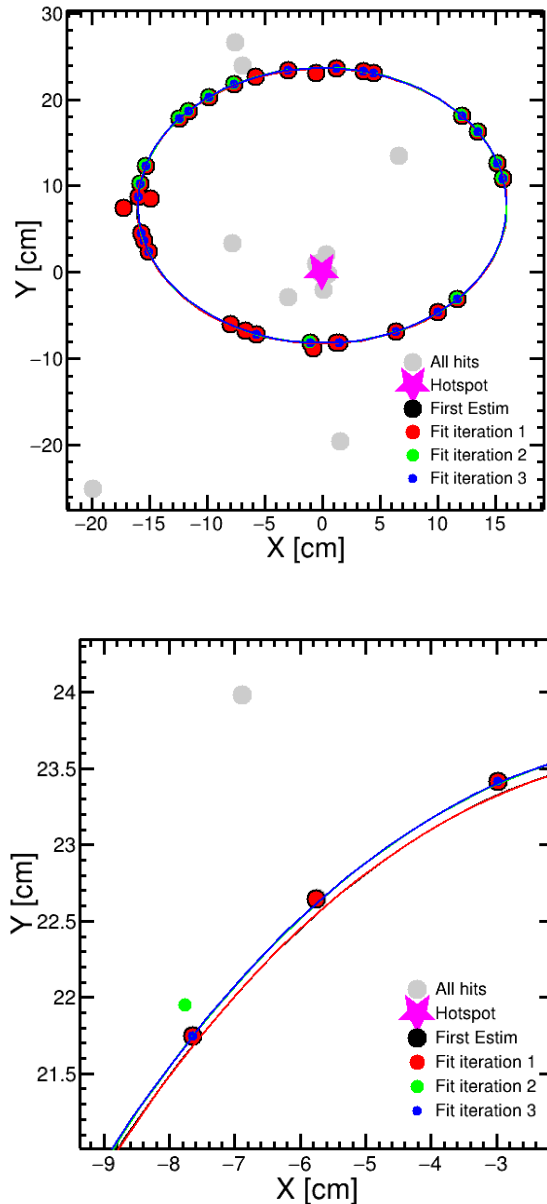


FIG. 3. Iterative elliptical fit on a typical distribution of detected Cherenkov photons hits (left). A zoomed view (right) of the same event is also shown. At every iteration, a different set of hits is pooled and the fit is adjusted.

distance is below threshold in the subsequent iterations. The procedure stops whenever for two subsequent iteration the same collocation of hits is selected, usually requiring 3-4 iterations. A minimum of 15 hits per fit is required to provide an accurate estimation of the the ellipse semi-axes reconstruction (i.e. $10 \mu\text{m}$) and only fits with a reduced χ^2 value lower than 3 are accepted in the analysis. These parameters were optimized on the trade-off between reconstruction accuracy and efficiency loss, the latter ranging from 30% to 45% with this final choice

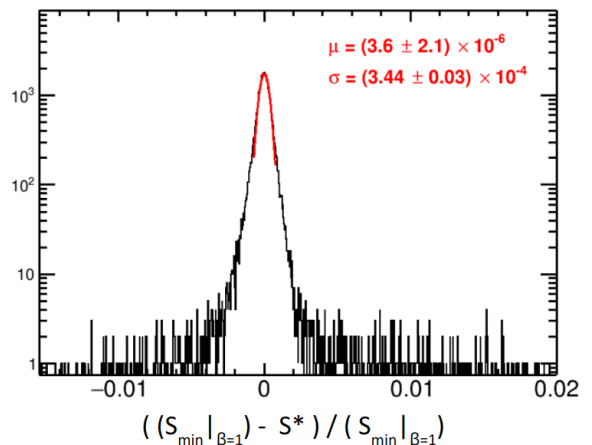


FIG. 4. The performance of the BDT calibration procedure evaluated as residual distribution of the BDT response (S^*) with respect to the regression target variable (minor semi-axis of the measured ellipse $S_{min|\beta=1}$) are shown. They are obtained with a test sample of $\beta \sim 1$ particles generated with generic inclinations (0° - 20°) and impact points on the radiator. The red curve represents a Gaussian fit of the core of the distribution.

of parameters.

Figure 3 shows the graphical rendering of the Cherenkov photon hits created by an high-energy (80 GeV/nucl) deuteron crossing the RICH detector and the elliptic fit performed on them. The minor semiaxis $S_{min} = \min\{S_A, S_B\}$ depends both from particle β and particle trajectory. These two relations are in very good approximation independent between each other and can be factored out. Thanks to this fact, by knowing the value that S_{min} assumes at $\beta \approx 1$ for every possible trajectory ($S_{min|\beta=1}$), it is possible to calibrate the instrument for the general $\beta < 1$ case. This calibration was accomplished using a machine learning (ML) approach, based on Boosted Decision Tree (BDT) technique [34].

A BDT regression model was trained using the ROOT TMVA Toolkit [35] on a mixture of $\beta \sim 1$ ($E_k = 200$ GeV/nucl.) $Z = 1$ particles, specifically p and D. The particles were uniformly generated from the top of the radiator plane with a continuous distribution of inclination angles relative to the detection plane. To build the training set, the Cherenkov ellipses generated by the particles are fitted with the procedure described above and for each the $S_{min|\beta=1}$ parameter is estimated. The BDT was trained to model the relation between $S_{min|\beta=1}$ and the trajectory of the particle, and to predict an S^* value targeting $S_{min|\beta=1}$ using a set of variables maximally independent from the velocity of the particle. These input variables were derived from the particle trajectory reconstructed using the first two silicon layers of the MSIS and include the impact point on the radiator, the track inclination, and the incidence angle of the particle on the spherical mirror. Figure 4 illustrates the performance of

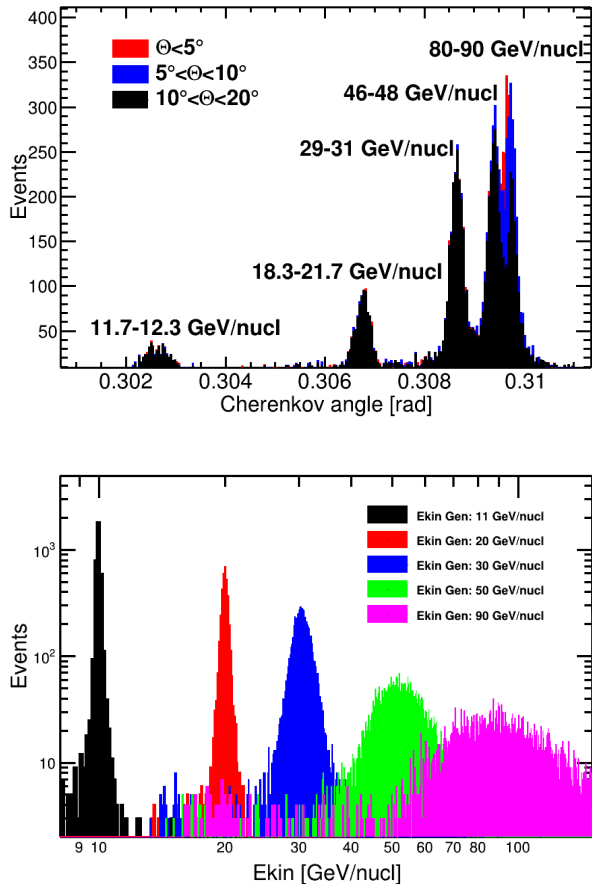


FIG. 5. Top: Distributions of reconstructed Cherenkov angles for samples of p and D generated at different energies with generic inclinations Θ [0° - 20°] and impact points on the radiator. Different colors represent different intervals of inclination of the incoming particle. Bottom: Distribution of measured E_k for mono-energetic samples of p and D generated with generic inclinations Θ [0° - 20°] and impact points on the radiator. Different colors represent different particle energies.

this on an independent test dataset simulated under conditions identical to those of the training set. The residuals between the value S^* predicted by the BDT and the target variable $S_{min}|_{\beta=1}$ on the test dataset exhibit a Gaussian-like distribution. A Gaussian fit to the core of this distribution yields $\sigma_{BDT} = 3.44 \times 10^{-4}$, corresponding to an uncertainty on S^* of $54.4 \mu\text{m}$. This value is comparable to the resolution on the S_{min} measurement. The S^* value obtained enables the normalization of $\beta < 1$ measurements, making them independent of track inclination and impact point.

The final performance of the RICH system and its reconstruction algorithm is shown in Figure 5, which depicts the results for protons and deuterons at various energies and generic impact point on the detector. No significant performance difference was found for the two par-

ticles. The total uncertainty observed in the Cherenkov angle measurement arises from multiple factors. These include the discretization of the RICH readout plane due to the finite size of the SiPM cells (see Appendix C), the imperfect focusing of the ellipse on the RICH plane (which dominates the σ_{BDT} uncertainty on S^*), and the contribution of the surface imperfections in the mirror. The resolution of the Cherenkov angle is nearly constant across the tested energy range, varying between 0.18 mrad and 0.22 mrad, and is compatible to the performance of other detectors with similar designs [36]. Thanks to the BDT-assisted calibration procedure, no significant dependence on the particle impact point and only minimal dependence on track inclination are shown in Figure 5 (top panel). The Figure also highlights a reduced selection efficiency from highly inclined particles which results in more eccentric ellipses.

IV. DESMO EXPECTED PERFORMANCES

The expected performance of DESMO were assessed with a simulation using the optimized design for cosmic D measurement. Monte Carlo simulations of p at different energies in the target E_k energy range were used to estimate the resolutions that can be obtained in the measurements of average displacement and E_k . The results of this study are reported in Figure 6. The E_k resolution is almost constant below 20 GeV/nucI with values from 0.1 % to 0.3 %. At higher energies it shows a parabolic trend, up to 25 % at 100 GeV/nucI. To minimize the bin-to-bin migration we divide the target energy range in 6 bins of increasing width, because of the degradation of the E_k resolution. The resolution in the displacement measurement as a function of proton momentum is compared to the theoretical trend obtained combining the average displacement resolution calculated in Appendix B (Equation B1 and Equation B2). The linearly rising trend at high energy, which falls outside the target energy range of DESMO, is where the overall displacement resolution starts to be importantly limited by the spatial resolution σ_x of the detection plane. Consequently, the displacement resolution results in the range from 21% to 23%.

To evaluate the D/p separation performance, a GEANT simulation of the apparatus was performed with equal number D and p particles generated in an uniform E_k distribution in the target energy range and different incidence angles in the range 0° - 20° . The separation between the two populations can be observed in Figure 7. The inverse displacement $1/d$, measured in mm^{-1} and proportional to particle momentum, was chosen as the separation variable for the analysis. This allows to compress the distribution of p and expand the distribution of the less abundant D, making the separation between the two when using realistic abundances more visible. A similar simulation, with D and p events generated with an isotropic angular distribution from a square surface of

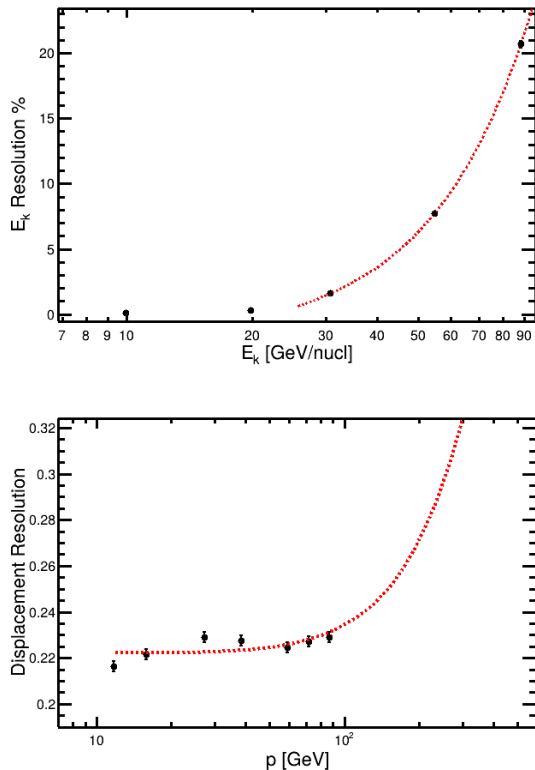


FIG. 6. Top: Resolution in the E_k measurement by the DESMO RICH as a function of true E_k . A parabolic trend is superimposed to data to guide the eye (red dashed curve). Bottom: Resolution of the measurement of the average displacement performed by DESMO for protons, as a function of particle momentum p , compared with the theoretical expectations discussed in the text for an optimized prototype with 9 stations (red dashed curve).

$1 \times 1 \text{ m}^2$ placed above the detector, was used to estimate the detector acceptance. Only particles which create a Cherenkov reconstructed ring with the quality requirements discussed in Section III B and with a valid displacement measurement obtained by all of the measuring stations are accepted.

The angular view of the detector design is limited and it is possible to measure particles with $\sim 18^\circ$ maximum inclination. This, combined with the efficiency of the selections described above, results in a almost constant acceptance of $\sim 40 \text{ cm}^2 \text{ sr}$ in the overall energy range.

Finally, the capabilities of the DESMO detector in D/p separation were evaluated simulating a realistic cosmic mixture of D and p, with a power-law spectrum in E_k ($\propto E_k^{-2.7}$) and constant D abundance of 2.5 % in 10-100 GeV/nuc E_k range. The total number of simulated events was chosen taking into account the total statistic attainable with the acceptance of the DESMO detector during a total exposure time of 60 days, achievable with a couple of balloon flights of 30 days each. The simulated events passing the quality selection were collected

in the 6 measured E_k bins of the analysis and for each bin the $1/d$ distribution was evaluated. The distributions were fitted using p and D templates obtained from independent simulations using the ROOT MINUIT2 [37] minimization algorithm. The results of the fit procedure for every E_k bin are shown in Figure 8. As can be seen, with the simulated isotopic abundances, the p distribution alone is never sufficient to explain the observed distribution in simulated data. The D shoulder is always visible and it is possible to extract the D/p fraction from each of the bins. The measured D/p fraction from this simulation is shown in Figure 9. As can be seen, although with a small systematic difference at the lowest energies, DESMO is able to measure the D relative abundance in good agreement with the injected ratio across the whole energy range. The results of these evaluation show a precision of the order of 5-8 % on the D/p ratio, taking in account only the statistical uncertainty from the fit.

The precise evaluation of the systematic uncertainty given by the fragmentation of D and heavier nuclei such as ^4He in (a) the residual atmosphere above the detector and (b) in the detector itself is beyond the purpose of this work. Uncertainty (a) is expected to be in the 2-5% range [38], and uncertainty (b) to be below 5% [6]. These uncertainty estimations are a clear indication that a D abundance of the order of 1-2% in the cosmic Hydrogen can be significantly detected by DESMO at energies up to 100 GeV/nuc. All the aforementioned studies demonstrate the effectiveness of DESMO on addressing his primary physics target. In addition, its measurement technique could be easily adapted to address other interesting cosmic-ray measurements. In Appendix A, we outline some of the most promising ones, accessible by DESMO directly or by upgraded versions of its design.

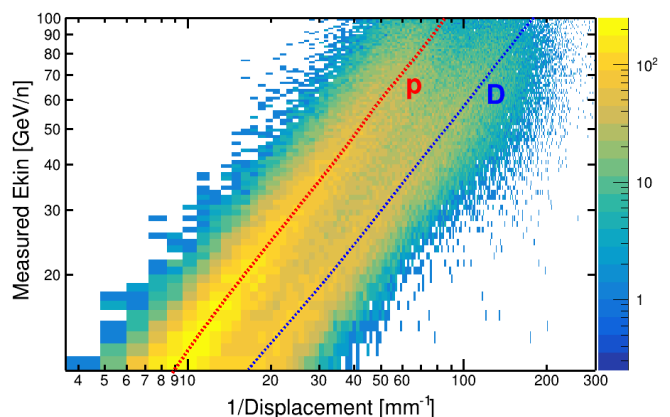


FIG. 7. The distribution of measured E_k versus measured inverse average displacement obtained by the DESMO prototype, for simulated events of D and p. The red and blue dotted lines represents respectively the theoretical expected behavior for protons and D nuclei.

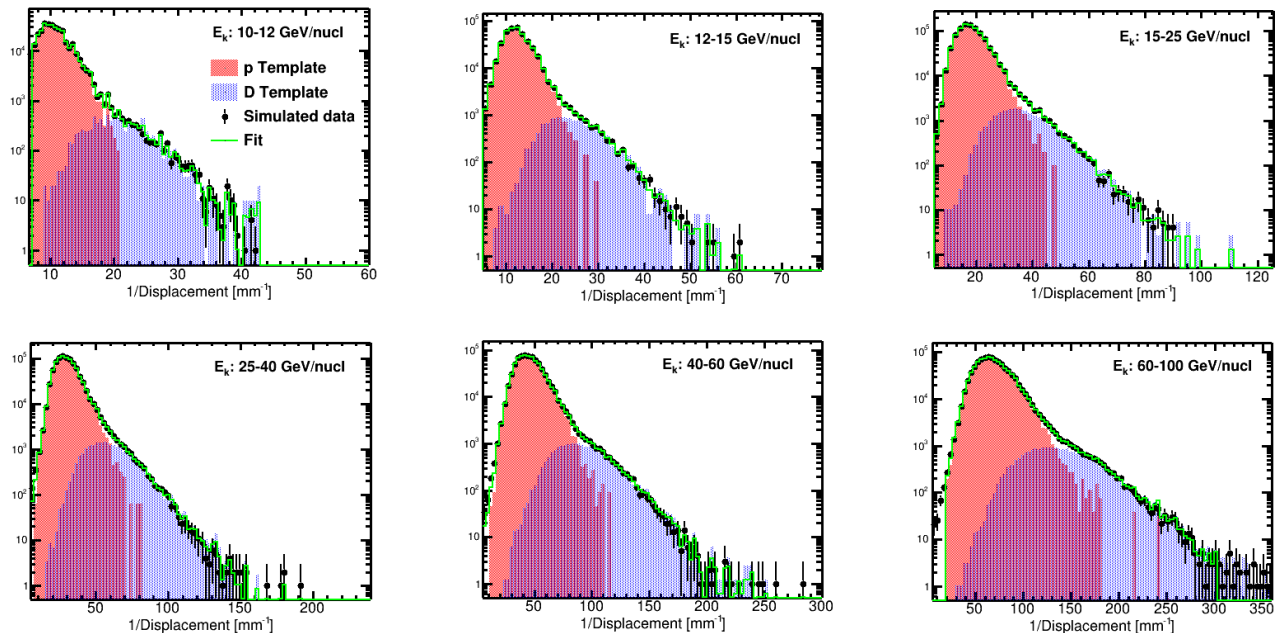


FIG. 8. Template fits of the inverse displacement distributions obtained from 60 days simulated cosmic Hydrogen flux, using the hypothesis of D abundance discussed in the text, in the six E_k intervals measurable by DESMO.

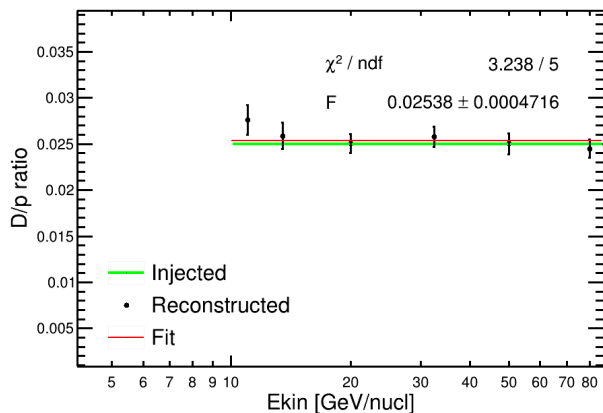


FIG. 9. Reconstructed D/p abundance detectable by a 60 days DESMO experiment on a simulated cosmic Hydrogen flux compared with the D fraction injected in the simulation (green solid line). Error bars represent statistical uncertainty from the template fit. A constant fit (red continuous line) on the reconstructed data yields a ratio F compatible with the injected one.

V. CONCLUSION

Studying the flux of cosmic-ray Deuterium (D) is a way to probe the mechanisms of cosmic-ray (CR) propagation and offers a unique insight into several topics: the investigation of the spallation processes, the composition of the interstellar medium (ISM), and the physi-

cal laws governing the CR diffusion. Deuterium, compared to heavier secondary species, with its light mass, enables to study the CR propagation over larger galactic distances. Additionally, its production from light primaries like ^4He provides a complementary perspective to heavier secondary-to-primary ratios such as B/C.

The recent observations from the AMS02 experiment questioned our understating on these matters, challenging the traditional view of Deuterium as a purely secondary species. Its high-energy spectrum appears significantly harder than expected, resembling the one of protons, but deviating notably from the secondary ^3He . This suggests the existence of a primary-like Deuterium component, raising fundamental questions about CR propagation and about the universality postulate of CR diffusion. Understanding these deviations has implications not only with regards of cosmic-ray propagation, but also for indirect Dark Matter searches, since it helps to constrain the \bar{D} , a promising and nearly background-free channel.

In this work, we scrutinized the current knowledge about high-energy Deuterium, derived from the available experimental measurements and theoretical models. The emerging picture is complex, and its interpretation remains debated. Despite the precision measurements provided by AMS02 up to 21 GV, which hint toward a primary-like component, recent high-profile theoretical studies have shown that it is possible to explain this within a secondary framework. However, the large uncertainties in the nuclear cross sections and diffusion parameters still leave room for discussion on the theoretical side. Moreover, independent experimental results from

SOKOL and CAPRICE98 show a significantly high Deuterium flux at high rigidities, which is difficult to contextualize within a secondary production scenario.

To shed light on this topic a high-precision flux measurement, beyond the currently explored energy range, is required. This challenge could be addressed with DESMO (DEuterio con Scattering MultiplO), a balloon-borne experiment designed to measure the deuteron flux in the 20–200 GV rigidity range. DESMO leverages on a new experimental technique for the measurement of cosmic deuteron (D) flux at high energies. Matching stringent requirements on cost and complexity, it was designed to be operated as a particularly lightweight (~ 90 kg), relatively small ($60 \times 60 \times 150$ cm³) and robust balloon-borne experiment, focused to explore the isotopic composition of the CR Hydrogen with a precision never reached before. In this work we showed the performance of DESMO in distinguishing D, achieving a few percent level precision in the measurement of the D/p fraction, using a template-fit approach. Such performance, given the DESMO acceptance of 40 cm² sr, is attainable with a limited exposure time (60 days). The proposed DESMO design meets all feasibility requirements described in the paper and could enable a fundamental measurement capable of revealing the true nature of cosmic-ray Deuterium.

ACKNOWLEDGEMENTS

We would like to express our gratitude to Dr. Francesco Nozzoli for the insightful discussions and for the bibliographic support. We also want to thank the referee for the useful comments and suggestions.

Appendix A: Different scientific scenarios

Beyond delivering a deuteron flux measurement, DESMO also serves as a proof of concept for its novel measurement technique, which could be adopted for future applications.

In this section, following the same approach that led the design of DESMO, we outline various physics measurements achievable with minimal modifications to DESMO’s design, or in the last most ambitious case, with the introduction of an additional module:

- **Gamma ray burst detection:** High-energy gamma-rays can convert in the target material of DESMO, producing electron-positron pairs detectable by the following PPT modules. Electron-positron pair can also be easily measured by the DESMO BGO targets, which can effectively act as an electromagnetic calorimeter. The segmentation of the BGO targets and the signals of the silicon pixels would allow a 3D reconstruction of the electromagnetic shower and its distinction from hadronic ones. The absence of a signal in RICH will provide rejection against electron background and further anti-coincidence for hadrons. Only the elaboration of advanced track analysis techniques are required to address this measurement.
- **Low-Energy anti-protons flux measurement:** By precisely balancing the amount of target material of DESMO, low-energy anti-proton annihilation can be induced. The resulting pion star from \bar{p} annihilation is easily detectable by tracking planes of DESMO, providing a signature for anti-protons below 0.2 GeV/nucleon.
- **Cosmic \bar{D} detection:** Detecting even a few confirmed anti-deuteron (\bar{D}) events would be a groundbreaking discovery in cosmic-ray physics, as it would provide strong evidence of annihilating DM in the galactic halo [12, 39]. The expected \bar{D} signal, concentrated at energies below 1 GeV/nucleon, is extremely rare, with fluxes below 10^{-5} m² sec sr GeV/nucleon [40], and faces significant background interference from anti-protons (\bar{p}). Current and future large-scale experiments like AMS02 [41] and ALADINO [42] have the potential to detect these signals, but specialized detectors such as the General Anti-Particle Spectrometer (GAPS) are also in an advanced developmental phase. As shown in Section B2 of the Appendix, the MSIS detector can be optimized for low energy studies, and for such can be shortened by a factor up to three, increasing its acceptance by a factor of 10 or more. The DESMO design described in this work cannot perform nuclei/anti-nuclei discrimination, since neither MSIS nor RICH can distinguish charge sign of the incoming particle. With the addition of a new module to the design, a $35 \times 35 \times 35$ cm³ BGO

calorimeter (CALO) matter/anti-matter discrimination and further distinction of \bar{D} from \bar{p} can be achievable. Moreover, replacing BGO as the target material in MSIS with faster high density scintillating crystals like Gadolinium Aluminium Gallium Garnet (GAGG) could also enable time-of-flight (TOF) measurements to determine particle velocity. The RICH would provide further anti-coincidence for high energy events. This modified design, with a total mass under 400 kg (dominated by CALO), remains well-suited for long-duration high-altitude polar balloon flights. The \bar{D} experimental signature mirrors that of a similar-energy deuteron in MSIS and RICH but features a significantly higher energy deposit in CALO due to annihilation energy release. The mass difference relative to anti-protons \bar{p} results in smaller displacements in MSIS and greater energy release in CALO, enabling \bar{p}/\bar{D} distinction.

We acknowledge that the proposed improvements to the DESMO detector and its applicability to other experimental scenarios discussed in this section (especially regarding the cosmic \bar{D} detection) require further detailed studies.

Appendix B: Optimization of MSIS design

The performances of the MSIS detector described in Section III A in distinguishing isotopes of the same velocity fundamentally depend on 4 design parameters:

- target width x ;
- distance between subsequent PPT modules S ;
- spacing between the silicon planes of the PPT modules L ;
- number of measuring stations N .

It is possible to attempt an optimization of the MSIS design starting given the design limits specified in Section III and using:

$$\Theta_{MS} = \frac{13.6 \text{ MeV}}{\beta p} z \sqrt{x/X_0} \left[1 + 0.038 \ln \left(\frac{x}{X_0} \right) \right] \quad (\text{B1})$$

where the average scattering angle, Θ_{MS} , depends on the particle's charge z and momentum p and on the thickness x of the material, with radiation length X_0 [43].

The distribution of trajectory deviations θ given by a single PPT module can be approximated to a gaussian distribution with $\sigma = \theta_{MS}$. Since only positive deviations from the trajectory measured by the precedent

PPT module are measured, the average measured can be expressed as:

$$\langle \theta \rangle = \int_0^\infty \theta \frac{1}{\theta_{MS} \sqrt{2\pi}} e^{-\frac{\theta^2}{2\theta_{MS}^2}} d\theta = \theta_{MS} \sqrt{\frac{2}{\pi}}$$

similarly, one can obtain the RMS value of the deviation from:

$$\langle \theta^2 \rangle = \int_0^\infty \theta^2 \frac{1}{\theta_{MS} \sqrt{2\pi}} e^{-\frac{\theta^2}{2\theta_{MS}^2}} d\theta = \theta_{MS}^2$$

and finally obtain the expected deviation distribution width σ_θ from the well known equation

$$\sigma_\theta^2 = \langle \theta^2 \rangle - \langle \theta \rangle^2$$

which represents the intrinsic uncertainty of the MS induced deviation measurement.

Such uncertainty needs to be combined with the spatial uncertainty σ_x of the hit position measurement and to the uncertainty on the position of the track interpolation $\sigma_I = \sqrt{2}(S/L)\sigma_x$ to obtain the final expression for the resolution on the average displacement resolution measured by N subsequent stations:

$$\frac{\sigma_d}{d} = \frac{1}{\theta_{MS} \sqrt{N}} \sqrt{\sigma_\theta^2 + \sigma_x^2 \left(\frac{1}{S^2} + \frac{2}{L^2} \right)} \quad (\text{B2})$$

Being S and L bound by $S+L=L_{TOT}/N$, where L_{TOT} is the total length of the MSIS detector, the Expression B2 has a minimum for $L=S \approx L_{TOT}/(2N)$. Besides L_{TOT} , Expression B2 has also a dependence on the width of the target hidden in the θ_{MS} parameter, but the limits on the overall mass and length of the total detector discussed in Section III bound both of them, leaving only the number of stations N as a free parameter for the design optimization.

1. Nominal use case ($E > 10 \text{ GeV/nuc}$)

The predicted displacement resolution was calculated as a function of N and particle E_k , for ten different energies in the target energy range of the detector ($10 \leq E_k \leq 100 \text{ GeV/nuc}$). Figure 10 shows the results of this calculation. From the Figure it is visible that the curves at all the energies follow the general $\propto 1/\sqrt{N}$ trend. For higher energies and large values of N the impact of the spatial resolution becomes important, because since $L + S$ is fixed, stations become shorter and shorter and a smaller displacement can be achieved ($d \propto S$). In particular, the same Figure shows also that designs with higher N approach the limit in which the displacement at higher energy become comparable to the spatial resolution of the tracking planes. A design with $N = 8$ was chosen as the best compromise that optimizes the displacement

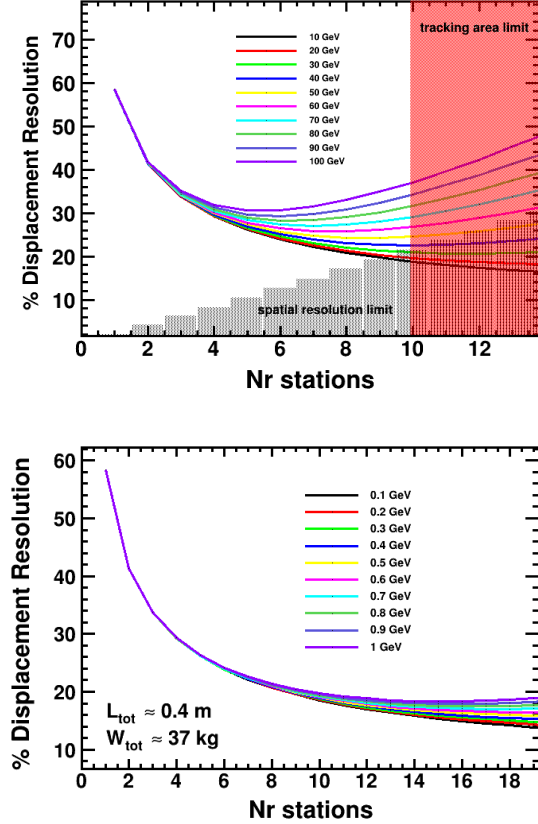


FIG. 10. Top: Resolution on average proton displacement measurement (σ_d/d) expected (in %) as a function of the number of PPT stations, considering an approximate total MSIS length of ~ 1 m and a total weight of ~ 90 kg. The red area corresponds to a total tracking area ≥ 2 m². The grey area corresponds to displacements at maximum E_k below the spatial resolution of the silicon planes. Bottom: Resolution on average proton displacement measurement (σ_d/d) expected (in %) as a function of the number of PPT stations, for different E_k below 1 GeV/nucl, for a different MSIS prototype optimized for low energy studies.

resolution across the whole energy range, still respecting the requirement on the total tracking area. This results in a final prototype with $x=9$ mm (included in S), $L=6$ cm, $S=6$ cm and thus $L_{PPT}=12$ cm, for a total detector weight ~ 90 kgm length ~ 1 m, and tracking area below 1.5 m².

2. Low energy case ($E \leq 1$ GeV/nucl)

The same calculation can be used to devise a possible design optimized for the sub-GeV energies. In this case

Equation B1 predicts much higher displacements, so the need for relatively high values of L_{PPT} is less stringent. This fact can be exploited to obtain a shorter detector, effectively increasing the overall acceptance by a factor 10 or more at parity of all the other metrics. Likewise, also the thickness of the Pb targets can be reduced, obtaining a much lighter and compact design. As an example, Figure 10 shows the displacement resolution as a function of N for a prototype with total length and target thickness (thus total weight) scaled by a factor of 0.5 with respect to the configuration described for the nominal use case. As can be seen, despite the smaller lever arm and target thickness, the measured displacements remain relatively large, such as the contribution of σ_θ remains basically negligible up to very high N for all the energies below 1 GeV/nucl.

As a result, for the low energy use case the most important limiting factor on the displacement resolution is the total tracking area.

Appendix C: Performances of RICH readout plane

SiPM chips are composed by elementary cells that are only partially sensitive to the incoming light. Each cell is in-fact characterized by a portion of dead area, due to the necessary coupling with the electronic readout. To estimate the performances of the RICH apparatus described in this work, a global Photon Detection Efficiency (PDE) can be defined, as:

$$PDE(\lambda, V) = \epsilon_Q(\lambda) \times P_T(V) \times \epsilon$$

where ϵ_Q is the quantum efficiency for converting photons to electron-hole pairs in the active region, P_T is the probability of a Geiger avalanche triggered by the generated electron, and ϵ is the geometric efficiency, accounting for the ratio between active and inactive areas on the sensor. The PDE depends on the photon wavelength λ and bias voltage V , and in general, smaller cells provide better spatial resolution and timing performance, at the cost of a reduced geometric efficiency. For our preliminary estimation, we assume a cell size of 30×30 micrometers, giving a spatial resolution per coordinate of about $30 / \sqrt{(12)} \mu\text{m} \approx 10 \mu\text{m}$. Under these conditions, literature shows that PDE values range from 20-60% [31]. For the performance estimation discussed in this work, an averaged value of 30% was chosen for PDE, accounting for all aforementioned factors. In this study, this value is approximated to be independent from the the effect of photons inclination and wavelength. A more refined performance estimation, including a realistic variability of the PDE under these parameters is beyond the scope of this study.

[1] Coste, B., Derome, L., Maurin, D., and Putze, A. Con-

straining galactic cosmic-ray parameters with $z \leq 2$ nu-

- clei. *A&A*, 539:A88, 2012.
- [2] Yoann Génolini, David Maurin, Igor V. Moskalenko, and Michael Unger. Current status and desired precision of the isotopic production cross sections relevant to astrophysics of cosmic rays: Li, Be, B, C, and N. *Phys. Rev. C*, 98:034611, Sep 2018.
- [3] Andrew W. Strong and Igor V. Moskalenko. Propagation of cosmic-ray nucleons in the galaxy. *The Astrophysical Journal*, 509(1):212, Dec 1998.
- [4] Nicola Tomassetti and Jie Feng. The curious case of high-energy deuterons in galactic cosmic rays. *The Astrophysical Journal Letters*, 835(2):L26, Jan 2017.
- [5] Nicola Tomassetti. Solar and nuclear physics uncertainties in cosmic-ray propagation. *Phys. Rev. D*, 96:103005, Nov 2017.
- [6] M. Aguilar, B. Alpat, G. Ambrosi, H. Anderson, L. Arruda, N. Attig, C. Bagwell, F. Barao, M. Barbanera, L. Barrin, A. Bartoloni, R. Battiston, A. Bayyari, N. Belyaev, B. Bertucci, V. Bindi, K. Bollweg, J. Bolster, M. Borchiellini, B. Borgia, M. J. Boschini, M. Bourquin, C. Brugnoli, J. Burger, W. J. Burger, X. D. Cai, M. Capell, J. Casaus, G. Castellini, F. Cervelli, Y. H. Chang, G. M. Chen, G. R. Chen, H. Chen, H. S. Chen, Y. Chen, L. Cheng, H. Y. Chou, S. Chouridou, V. Choutko, C. H. Chung, C. Clark, G. Coignet, C. Consolandi, A. Contin, C. Corti, Z. Cui, K. Dadzie, F. D'Angelo, A. Dass, C. Delgado, S. Della Torre, M. B. Demirköz, L. Derome, S. Di Falco, V. Di Felice, C. Díaz, F. Dimiccoli, P. von Doetinchem, F. Dong, F. Donnini, M. Duranti, A. Egorov, A. Eline, F. Faldi, D. Fehr, J. Feng, E. Fiandrini, P. Fisher, V. Formato, C. Gámez, R. J. García-López, C. Gargiulo, H. Gast, M. Gervasi, F. Giovacchini, D. M. Gómez-Coral, J. Gong, D. Grandi, M. Graziani, A. N. Guracho, S. Haino, K. C. Han, R. K. Hashmani, Z. H. He, B. Heber, T. H. Hsieh, J. Y. Hu, B. W. Huang, M. Ionica, M. Incagli, Yi Jia, H. Jinchi, G. Karagöz, S. Khan, B. Khiali, Th. Kirn, A. P. Klipfel, O. Kounina, A. Kounine, V. Koutsenko, D. Krasnopevtsev, A. Kuhlman, A. Kulemin, G. La Vacca, E. Laudi, G. Laurenti, G. LaVecchia, I. Lazzizzera, H. T. Lee, S. C. Lee, H. L. Li, J. Q. Li, M. Li, M. Li, Q. Li, Q. Li, Q. Y. Li, S. Li, S. L. Li, J. H. Li, Z. H. Li, M. J. Liang, P. Liao, C. H. Lin, T. Lippert, J. H. Liu, P. C. Liu, S. Q. Lu, Y. S. Lu, K. Luebelsmeyer, J. Z. Luo, Q. Luo, S. D. Luo, Xi Luo, C. Mañá, J. Marín, J. Marquardt, G. Martínez, N. Masi, D. Maurin, T. Medvedeva, A. Menchaca-Rocha, Q. Meng, V. V. Mikhailov, M. Molero, P. Mott, L. Musolin, Y. Najafi Jozani, R. Nicolaidis, N. Nikonov, F. Nozzoli, J. Ocampo-Peleteiro, A. Oliva, M. Orcinha, F. Palmonari, M. Panizza, A. Pashnin, M. Pauluzzi, S. Pensotti, P. Pietzcker, V. Plyaskin, S. Poluianov, D. Pridöhl, Z. Y. Qu, L. Quadrani, P. G. Rancoita, D. Rapin, A. Reina Conde, E. Robyn, I. Rodríguez-García, L. Romaneehsen, F. Rossi, A. Rozhkov, D. Rozza, R. Sagdeev, E. Savin, S. Schael, A. Schultz von Dratzig, G. Schwing, E. S. Seo, B. S. Shan, A. Shukla, T. Siedenbarg, G. Silvestre, J. W. Song, X. J. Song, R. Sonnabend, L. Strigari, T. Su, Q. Sun, Z. T. Sun, L. Tabarroni, M. Tacconi, Z. C. Tang, J. Tian, Y. Tian, Samuel C. C. Ting, S. M. Ting, N. Tomassetti, J. Torsti, T. Urban, I. Usoskin, V. Vagelli, R. Vainio, M. Valencia-Otero, E. Valente, E. Valtonen, M. Vázquez Acosta, M. Vecchi, M. Velasco, C. X. Wang, L. Wang, L. Q. Wang, N. H. Wang, Q. L. Wang, S. Wang, X. Wang, Z. M. Wang, J. Wei, Z. L. Weng, H. Wu, Y. Wu, Z. B. Wu, J. N. Xiao, R. Q. Xiong, X. Z. Xiong, W. Xu, Q. Yan, H. T. Yang, Y. Yang, A. Yelland, H. Yi, Y. H. You, Y. M. Yu, Z. Q. Yu, C. Zhang, F. Z. Zhang, J. Zhang, J. H. Zhang, Z. Zhang, P. W. Zhao, C. Zheng, Z. M. Zheng, H. L. Zhuang, V. Zhukov, A. Zichichi, and P. Zucco. Properties of cosmic deuterons measured by the alpha magnetic spectrometer. *Phys. Rev. Lett.*, 132:261001, Jun 2024.
- [7] O. Adriani, G. C. Barbarino, G. A. Bazilevskaia, R. Bellotti, M. Boezio, E. A. Bogomolov, M. Bongi, V. Bonvicini, S. Bottai, A. Bruno, F. Cafagna, D. Campana, P. Carlson, M. Casolino, G. Castellini, C. De Donato, C. De Santis, N. De Simone, V. Di Felice, V. Formato, A. M. Galper, A. V. Karelin, S. V. Koldashov, S. Koldobskiy, S. Y. Krutkov, A. N. Kvashnin, A. Leonov, V. Malakhov, L. Marcelli, M. Martucci, A. G. Mayorov, W. Menn, M. Mergè, V. V. Mikhailov, E. Mocchiutti, A. Monaco, N. Mori, R. Munini, G. Osteria, F. Palma, B. Panico, P. Papini, M. Pearce, P. Picozza, M. Ricci, S. B. Ricciarini, R. Sarkar, V. Scotti, M. Simon, R. Sparvoli, P. Spillantini, Y. I. Stozhkov, A. Vacchi, E. Vannucini, G. Vasilyev, S. A. Voronov, Y. T. Yurkin, G. Zampa, and N. Zampa. Measurements of cosmic-ray hydrogen and helium isotopes with the Pamela experiment. *The Astrophysical Journal*, 818(1):68, Feb 2016.
- [8] P. Papini, S. Piccardi, P. Spillantini, E. Vannucini, M. Ambriola, R. Bellotti, F. Cafagna, F. Ciaccio, M. Circella, C. N. De Marzo, S. Bartalucci, M. Ricci, D. Bergström, P. Carlson, T. Francke, P. Hansen, E. Mocchiutti, M. Boezio, V. Bonvicini, P. Schiavon, A. Vacchi, N. Zampa, U. Bravar, S. J. Stochaj, M. Casolino, M. P. De Pascale, A. Morselli, P. Picozza, R. Sparvoli, M. Hof, J. Kremer, W. Menn, M. Simon, J. W. Mitchell, J. F. Ormes, S. A. Stephens, R. E. Streitmatter, and M. Suffert. High-Energy Deuteron Measurement with the CAPRICE98 Experiment. *Astrophys. J.*, 615(1):259–274, November 2004.
- [9] Andrey Turundaevskiy and Dmitry Podorozhnyi. High energy deuterons in cosmic rays registered by the Sokol satellite experiment. *Advances in Space Research*, 59(1):496–501, 2017.
- [10] K. M. V. Apparao. Flux of Cosmic Ray Deuterons with Rigidity Above 16.8 GV. In *Proceedings of the 13th International Conference on Cosmic Rays*, volume 1, page 126, Denver, Colorado, 1973. OG Sessions.
- [11] Qiang Yuan and Yi-Zhong Fan. The AMS-02 cosmic-ray deuteron flux is consistent with a secondary origin. *The Astrophysical Journal Letters*, 974(1):L14, Oct 2024.
- [12] F. Donato, N. Fornengo, and D. Maurin. Antideuteron fluxes from dark matter annihilation in diffusion models. *Phys. Rev. D*, 78:043506, Aug 2008.
- [13] Ryan J. Cooke, Max Pettini, and Charles C. Steidel. One percent determination of the primordial deuterium abundance*. *The Astrophysical Journal*, 855(2):102, Mar 2018.
- [14] A.E. Vladimirov, S.W. Digel, G. Jóhannesson, P.F. Michelson, I.V. Moskalenko, P.L. Nolan, E. Orlando, T.A. Porter, and A.W. Strong. Galprop webrun: An internet-based service for calculating galactic cosmic ray propagation and associated photon emissions. *Computer Physics Communications*, 182(5):1156–1161, 2011.
- [15] Xing-Jian Lv, Xiao-Jun Bi, Kun Fang, Peng-Fei Yin, and Meng-Jie Zhao. Cosmic-ray deuteron excess from a primary component, 2024.

- [16] DAMPE Collaboration, Q. An, R. Asfandiyarov, P. Azzarello, P. Bernardini, X. J. Bi, M. S. Cai, J. Chang, D. Y. Chen, H. F. Chen, J. L. Chen, W. Chen, M. Y. Cui, T. S. Cui, H. T. Dai, A. D'Amone, A. De Benedittis, I. De Mitri, M. Di Santo, M. Ding, T. K. Dong, Y. F. Dong, Z. X. Dong, G. Donvito, D. Droz, J. L. Duan, K. K. Duan, D. D'Urso, R. R. Fan, Y. Z. Fan, F. Fang, C. Q. Feng, L. Feng, P. Fusco, V. Gallo, F. J. Gan, M. Gao, F. Gargano, K. Gong, Y. Z. Gong, D. Y. Guo, J. H. Guo, X. L. Guo, S. X. Han, Y. M. Hu, G. S. Huang, X. Y. Huang, Y. Y. Huang, M. Ionica, W. Jiang, X. Jin, J. Kong, S. J. Lei, S. Li, W. L. Li, X. Li, X. Q. Li, Y. Li, Y. F. Liang, Y. M. Liang, N. H. Liao, C. M. Liu, H. Liu, J. Liu, S. B. Liu, W. Q. Liu, Y. Liu, F. Loparco, C. N. Luo, M. Ma, P. X. Ma, S. Y. Ma, T. Ma, X. Y. Ma, G. Marsella, M. N. Mazziotta, D. Mo, X. Y. Niu, X. Pan, W. X. Peng, X. Y. Peng, R. Qiao, J. N. Rao, M. M. Salinas, G. Z. Shang, W. H. Shen, Z. Q. Shen, Z. T. Shen, J. X. Song, H. Su, M. Su, Z. Y. Sun, A. Surdo, X. J. Teng, A. Tykhonov, S. Vitillo, C. Wang, H. Wang, H. Y. Wang, J. Z. Wang, L. G. Wang, Q. Wang, S. Wang, X. H. Wang, X. L. Wang, Y. F. Wang, Y. P. Wang, Y. Z. Wang, Z. M. Wang, D. M. Wei, J. J. Wei, Y. F. Wei, S. C. Wen, D. Wu, J. Wu, L. B. Wu, S. S. Wu, X. Wu, K. Xi, Z. Q. Xia, H. T. Xu, Z. H. Xu, Z. L. Xu, Z. Z. Xu, G. F. Xue, H. B. Yang, P. Yang, Y. Q. Yang, Z. L. Yang, H. J. Yao, Y. H. Yu, Q. Yuan, C. Yue, J. J. Zang, F. Zhang, J. Y. Zhang, J. Z. Zhang, P. F. Zhang, S. X. Zhang, W. Z. Zhang, Y. Zhang, Y. J. Zhang, Y. L. Zhang, Y. P. Zhang, Y. Q. Zhang, Z. Zhang, Z. Y. Zhang, H. Zhao, H. Y. Zhao, X. F. Zhao, C. Y. Zhou, Y. Zhou, X. Zhu, Y. Zhu, and S. Zimmer. Measurement of the cosmic ray proton spectrum from 40 gev to 100 tev with the dampe satellite. *Science Advances*, 5(9):eaax3793, 2019.
- [17] M. Aguilar, L. Ali Cavazonza, B. Alpat, G. Ambrosi, L. Arruda, N. Attig, S. Aupetit, P. Azzarello, A. Bachlechner, F. Barao, A. Barrau, L. Barrin, A. Bartoloni, L. Basara, S. Başğömez-du Pree, M. Battarbee, R. Battiston, U. Becker, M. Behlmann, B. Beischer, J. Berdugo, B. Bertucci, K. F. Bindel, V. Bindi, W. de Boer, K. Bollweg, V. Bonnivard, B. Borgia, M. J. Boschini, M. Bourquin, E. F. Bueno, J. Burger, W. J. Burger, F. Cadoux, X. D. Cai, M. Capell, S. Caroff, J. Casaus, G. Castellini, F. Cervelli, M. J. Chae, Y. H. Chang, A. I. Chen, G. M. Chen, H. S. Chen, L. Cheng, H. Y. Chou, E. Choumilov, V. Choutko, C. H. Chung, C. Clark, R. Clavero, G. Coignet, C. Consolandi, A. Contin, C. Corti, W. Creus, M. Crispoltoni, Z. Cui, K. Dadzie, Y. M. Dai, A. Datta, C. Delgado, S. Della Torre, O. Demakov, M. B. Demirköz, L. Derome, S. Di Falco, F. Dimiccoli, C. Díaz, P. von Doetinchem, F. Dong, F. Donnini, M. Duranti, D. D'Urso, A. Egorov, A. Eline, T. Eronen, J. Feng, E. Fiandrini, P. Fisher, V. Formato, Y. Galaktionov, G. Gallucci, R. J. García-López, C. Gargiulo, H. Gast, I. Gebauer, M. Gervasi, A. Ghelfi, F. Giovacchini, D. M. Gómez-Coral, J. Gong, C. Goy, V. Grabski, D. Grandi, M. Graziani, K. H. Guo, S. Haino, K. C. Han, Z. H. He, M. Heil, J. Hoffman, T. H. Hsieh, H. Huang, Z. C. Huang, C. Huh, M. Incagli, M. Ionica, W. Y. Jang, Yi Jia, H. Jinchi, S. C. Kang, K. Kanishev, B. Khiali, G. N. Kim, K. S. Kim, Th. Kirn, C. Konak, O. Kounina, A. Kounine, V. Koutsenko, A. Kulemzin, G. La Vacca, E. Laudi, G. Laurenti, I. Lazzizzera, A. Lebedev, H. T. Lee, S. C. Lee, C. Leluc, H. S. Li, J. Q. Li, Q. Li, T. X. Li, Y. Li, Z. H. Li, Z. Y. Li, S. Lim, C. H. Lin, P. Lipari, T. Lippert, D. Liu, Hu Liu, V. D. Lordello, S. Q. Lu, Y. S. Lu, K. Luebelsmeyer, F. Luo, J. Z. Luo, S. S. Lyu, F. Machate, C. Mañá, J. Marín, T. Martin, G. Martínez, N. Masi, D. Maurin, A. Menchaca-Rocha, Q. Meng, V. M. Mikuni, D. C. Mo, P. Mott, T. Nelson, J. Q. Ni, N. Nikonov, F. Nozzoli, A. Oliva, M. Orcinha, F. Palmonari, C. Palomares, M. Paniccia, M. Pauluzzi, S. Pensotti, C. Perrina, H. D. Phan, N. Picot-Clemente, F. Pilo, C. Pizzolotto, V. Plyaskin, M. Pohl, V. Poireau, L. Quadrani, X. M. Qi, X. Qin, Z. Y. Qu, T. Rähkä, P. G. Rancoita, D. Rapin, J. S. Ricol, S. Rosier-Lees, A. Rozhkov, D. Rozza, R. Sagdeev, S. Schael, S. M. Schmidt, A. Schulz von Dratzig, G. Schwering, E. S. Seo, B. S. Shan, J. Y. Shi, T. Siedenburger, D. Son, J. W. Song, M. Tacconi, X. W. Tang, Z. C. Tang, D. Tesaro, Samuel C. C. Ting, S. M. Ting, N. Tomassetti, J. Torsti, C. Türkoğlu, T. Urban, V. Vagelli, E. Valente, E. Valtonen, M. Vázquez Acosta, M. Vecchi, M. Velasco, J. P. Vialle, V. Vitale, S. Vitillo, L. Q. Wang, N. H. Wang, Q. L. Wang, X. Wang, X. Q. Wang, Z. X. Wang, C. C. Wei, Z. L. Weng, K. Whitman, H. Wu, X. Wu, R. Q. Xiong, W. Xu, Q. Yan, J. Yang, M. Yang, Y. Yang, H. Yi, Y. J. Yu, Z. Q. Yu, M. Zannoni, S. Zeissler, C. Zhang, F. Zhang, J. Zhang, J. H. Zhang, S. W. Zhang, Z. Zhang, Z. M. Zheng, H. L. Zhuang, V. Zhukov, A. Zichichi, N. Zimmermann, and P. Zuccon. Observation of the identical rigidity dependence of he, c, and o cosmic rays at high rigidities by the alpha magnetic spectrometer on the international space station. *Phys. Rev. Lett.*, 119:251101, Dec 2017.
- [18] Francesco Dimiccoli and Francesco Maria Follega. A multiple scattering-based technique for isotopic identification in cosmic rays. *Particles*, 7(2):477–488, 2024.
- [19] N Agafonova, A Aleksandrov, O Altinok, A Anokhina, S Aoki, A Ariga, T Ariga, D Autiero, A Badertscher, A Bagulya, A Ben Dhahbi, A Bertolin, M Besnier, C Bozza, T Brugière, R Brugnera, F Brunet, G Brunetti, S Buontempo, A Cazes, L Chaussard, M Chernyavskiy, V Chiarella, A Chukanov, N D'Ambrosio, F Dal Corso, G De Lellis, P del Amo Sanchez, Y Déclais, M De Serio, F Di Capua, A Di Crescenzo, D Di Ferdinando, N Di Marco, S Dmitrievski, M Dracos, D Duchesneau, S Dusini, T Dzhatdov, J Ebert, O Egorov, R Enikeev, A Ereditato, L S Esposito, J Favier, T Ferber, R A Fini, D Frekers, T Fukuda, A Garfagnini, G Giacomelli, M Giorgini, C Göllnitz, J Goldberg, D Golubkov, L Goncharova, Y Gornushkin, G Grella, F Grianti, A M Guler, C Gustavino, C Hagner, K Hamada, T Hara, M Hierholzer, A Hollnagel, K Hoshino, M Ieva, H Ishida, K Jakovcic, C Jollet, F Juget, M Kamiscioglu, K Kazuyama, S H Kim, M Kimura, N Kitagawa, B Klicek, J Knuesel, K Kodama, M Komatsu, U Kose, I Kreslo, H Kubota, C Lazzaro, J Lenkeit, I Lippi, A Ljubicic, A Longhin, P Loverre, G Lutter, A Malgin, G Mandrioli, K Manai, J Marteau, T Matsuo, V Matveev, N Mauri, E Medinaceli, F Meisel, A Meregaglia, P Migliozi, S Mikado, S Miyamoto, P Monacelli, K Morishima, U Moser, M T Muciaccia, N Naganawa, T Naka, M Nakamura, T Nakano, D Naumov, V Nikitina, K Niwa, Y Nonoyama, S Ogawa, N Okatava, A Olshevskiy, M Paniccia, A Paoloni, B D Park, I G Park, A Pastore, L Patrizii, E Pennacchio, H Pessard, K Pretzl, V Pilipenko, C Pistillo, N Polukhina, M Poz-

- zato, F Pupilli, R Rescigno, T Roganova, H Rokujo, G Romano, G Rosa, I Rostovtseva, A Rubbia, A Russo, V Rzasny, O Ryazhskaya, O Sato, Y Sato, A Schembri, W Schmidt-Parzefall, H Schroeder, L Scotto Lavina, A Sheshukov, H Shibuya, G Shoziyoev, S Simone, M Sioli, C Sirignano, G Sirri, J S Song, M Spinetti, L Stanco, N Starkov, M Stipcevic, T Strauss, P Strolin, S Takahashi, M Tenti, F Terranova, I Tezuka, V Tioukov, P Tolun, A Trabelsi, T Tran, S Tufanli, P Vilain, M Vladimirov, L Votano, J L Vuilleumier, G Wilquet, B Wonsak, V Yakushev, C S Yoon, T Yoshioka, J Yoshida, Y Zaitsev, S Zemskova, A Zghiche, and R Zimmermann. Momentum measurement by the multiple coulomb scattering method in the opera lead-emulsion target. *New Journal of Physics*, 14(1):013026, jan 2012.
- [20] S. Agostinelli et al. GEANT4—a simulation toolkit. *Nucl. Instrum. Meth. A*, 506:250–303, 2003.
- [21] M. Mager. Alpile, the monolithic active pixel sensor for the alice its upgrade. *Nuclear Instruments and Methods in Physics Research Section A Accelerators Spectrometers Detectors and Associated Equipment*, 824:434–438, 07 2016.
- [22] Ester Ricci. A pixel based tracker for the HEPD-02 detector. *PoS, ICRC2023*:164, 2024.
- [23] Umberto Savino. Expected performance of the high energy particle detector (hepd-02) tracking system on board of the second china seismo-electromagnetic satellite. *Nuclear Instruments and Methods in Physics Research Section A: Accelerators, Spectrometers, Detectors and Associated Equipment*, 1063:169281, 03 2024.
- [24] Mohammad Farukhi. Bi4ge3o12 (bgo) - a scintillator replacement for nai(tl). *MRS Proceedings*, 16, 01 2011.
- [25] M. Mager. Alpile, the monolithic active pixel sensor for the alice its upgrade. *Nuclear Instruments and Methods in Physics Research Section A: Accelerators, Spectrometers, Detectors and Associated Equipment*, 824:434–438, 2016. Frontier Detectors for Frontier Physics: Proceedings of the 13th Pisa Meeting on Advanced Detectors.
- [26] Ivan N. Vuchkov and Lidia N. Boyadjieva. *Statistical Methods for Data Analysis*, pages 14–95. Springer Netherlands, Dordrecht, 2001.
- [27] Georg Viehhauser and Tony Weidberg. *Detectors in Particle Physics: A Modern Introduction*. CRC Press, 1st edition, 2024.
- [28] P Wang, A Beck, W Korner, H Scheller, and J Fricke. Density and refractive index of silica aerogels after low- and high-temperature supercritical drying and thermal treatment. *Journal of Physics D: Applied Physics*, 27(2):414, feb 1994.
- [29] F. Giovacchini. The RICH detector of the AMS-02 experiment aboard the International Space Station. *Nucl. Instrum. Meth. A*, 1055:168434, 2023.
- [30] RUI PEREIRA and on behalf of the AMS RICH collaboration. *The RICH detector of the AMS-02 experiment: status and physics prospects*, pages 901–905. World Scientific, 2008.
- [31] G. Ambrosi, M. Ambrosio, C. Aramo, B. Bertucci, E. Bissaldi, M. Bitossi, A. Boiano, C. Bonavolontà, M. Capasso, A. Circiello, L. Consiglio, D. Depaoli, F. Di Pierro, L. Di Venere, E. Fiandrini, N. Giglietto, F. Giordano, S. Incardona, M. Ionica, F. Licciulli, S. Loporchio, G. Marsella, V. Masone, F.R. Pantaleo, R. Paoletti, B. Ruggiero, A. Rugliancich, P. Silvestrini, L. Stiaccini, J. Tasseva, L. Tosti, G. Tripodo, V. Vagelli, and M. Valentino. High-density near-ultraviolet silicon photomultipliers: Characterization of photosensors for cherenkov light detection. *Nuclear Instruments and Methods in Physics Research Section A: Accelerators, Spectrometers, Detectors and Associated Equipment*, 1049:168023, 2023.
- [32] A. R. Altamura, A. Di Mauro, E. Nappi, N. Nicassio, M. van Emmerik, and G. Volpe. Aerogel characterization for RICH applications. In *9th International Workshop on Advances in Sensors and Interfaces*, 6 2023.
- [33] E. Cisbani, S. Colilli, R. Crateri, F. Cusanno, R. Fratoni, S. Frullani, F. Garibaldi, F. Giuliani, M. Gricia, M. Iodice, R. Iommi, M. Lucentini, A. Mostarda, L. Pierangeli, F. Santavenero, G.M. Urciuoli, R. De Leo, L. Lagamba, E. Nappi, A. Braem, and P. Vernin. Lightweight spherical mirrors for cherenkov detectors. *Nuclear Instruments and Methods in Physics Research Section A: Accelerators, Spectrometers, Detectors and Associated Equipment*, 496(2):305–314, 2003.
- [34] Yann Coadou. Boosted decision trees and applications. *EPJ Web of Conferences*, 55:02004–, 07 2013.
- [35] Jan Therhaag. TMVA Toolkit for multivariate data analysis in ROOT. *PoS, ICHEP2010*:510, 2010.
- [36] S.A. Wotton. The lhcb rich upgrade for the high luminosity lhcb era. *Nuclear Instruments and Methods in Physics Research Section A: Accelerators, Spectrometers, Detectors and Associated Equipment*, 1058:168824, 2024.
- [37] M. Hatlo, F. James, P. Mato, L. Moneta, M. Winkler, and A. Zsenei. Developments of mathematical software libraries for the LHC experiments. *IEEE Trans. Nucl. Sci.*, 52:2818–2822, 2005.
- [38] J. Z. Wang, E. S. Seo, K. Anraku, M. Fujikawa, M. Imori, T. Maeno, N. Matsui, H. Matsunaga, M. Motoki, S. Orito, T. Saeki, T. Sanuki, I. Ueda, K. Yoshimura, Y. Makida, J. Suzuki, K. Tanaka, A. Yamamoto, T. Yoshida, T. Mitsui, H. Matsumoto, M. Nozaki, M. Sasaki, J. Mitchell, A. Moiseev, J. Ormes, R. Streitmatter, J. Nishimura, Y. Yajima, and T. Yamagami. Measurement of cosmic-ray hydrogen and helium and their isotopic composition with the bess experiment. *The Astrophysical Journal*, 564(1):244, jan 2002.
- [39] T. Aramaki, S. Boggs, S. Bufalino, L. Dal, P. von Doetinchem, F. Donato, N. Fornengo, H. Fuke, M. Grefe, C. Hailey, B. Hamilton, A. Ibarra, J. Mitchell, I. Mognet, R.A. Ong, R. Pereira, K. Perez, A. Putze, A. Raklev, P. Salati, M. Sasaki, G. Tarle, A. Urbano, A. Vittino, S. Wild, W. Xue, and K. Yoshimura. Review of the theoretical and experimental status of dark matter identification with cosmic-ray antideuterons. *Physics Reports*, 618:1–37, 2016. Review of the theoretical and experimental status of dark matter identification with cosmic-ray antideuterons.
- [40] Carolin B. Brauning and Marco Cirelli. Anti-deuterons from heavy Dark Matter. *Phys. Lett. B*, 678:20–31, 2009.
- [41] Francesca Giovacchini and V. Choutko. Cosmic Rays Antideuteron Sensitivity for AMS-02 Experiment. In *30th International Cosmic Ray Conference*, volume 4, pages 765–768, 2008.
- [42] Oscar Adriani, Corrado Altomare, Giovanni Ambrosi, Philipp Azzarello, Felicia Carla Tiziana Barbato, Roberto Battiston, Bertrand Baudouy, Benedikt Bergmann, Eugenio Berti, Bruna Bertucci, Mirko Boezio, Valter Bonvicini, Sergio Bottai, Petr Burian, Mario Buscemi, Franck Cadoux, Valerio Calvelli, Donatella

- Campana, Jorge Casaus, Andrea Contin, Raffaello D'Alessandro, Magnus Dam, Ivan De Mitri, Francesco de Palma, Laurent Derome, Valeria Di Felice, Adriano Di Giovanni, Federico Donnini, Matteo Duranti, Emanuele Fiandrini, Francesco Maria Follega, Valerio Formato, Fabio Gargano, Francesca Giovacchini, Maura Graziani, Maria Ionica, Roberto Iuppa, Francesco Loparco, Jesús Marín, Samuele Mariotto, Giovanni Marsella, Gustavo Martínez, Manel Martínez, Matteo Martucci, Nicolò Masi, Mario Nicola Mazziotta, Matteo Mergé, Nicola Mori, Riccardo Munini, Riccardo Musenich, Lorenzo Mussolin, Francesco Nozzoli, Alberto Oliva, Giuseppe Osteria, Lorenzo Pacini, Mercedes Paniccchia, Paolo Papini, Mark Pearce, Chiara Perrina, Piergiorgio Picozza, Cecilia Pizzolotto, Stanislav Pospíšil, Michele Pozzato, Lucio Quadrani, Ester Ricci, Javier Rico, Lucio Rossi, Enrico Junior Schioppa, Davide Serini, Petr Smolyanskiy, Alessandro Sotgiu, Roberta Sparvoli, Antonio Surdo, Nicola Tomassetti, Valerio Vagelli, Miguel Ángel Velasco, Xin Wu, and Paolo Zuccon. Design of an antimatter large acceptance detector in orbit (aladino). *Instruments*, 6(2), 2022.
- [43] Particle Data Group, P A Zyla, R M Barnett, J Beringer, O Dahl, D A Dwyer, D E Groom, C J Lin, K S Lugovsky, E Pianori, D J Robinson, C G Wohl, W M Yao, K Agashe, G Aielli, B C Allanach, C Amisler, M Antonelli, E C Aschenauer, D M Asner, H Baer, Sw Banerjee, L Baudis, C W Bauer, J J Beatty, V I Belousov, S Bethke, A Bettini, O Biebel, K M Black, E Blucher, O Buchmuller, V Burkert, M A Bychkov, R N Cahn, M Carena, A Ceccucci, A Cerri, D Chakraborty, R Sekhar Chivukula, G Cowan, G D'Ambrosio, T Damour, D de Florian, A de Gouvêa, T DeGrand, P de Jong, G Dissertori, B A Dobrescu, M D'Onofrio, M Doser, M Drees, H K Dreiner, P Eerola, U Egede, S Eidelman, J Ellis, J Erler, V V Ezhela, W Fetscher, B D Fields, B Foster, A Freitas, H Gallagher, L Garren, H J Gerber, G Gerbier, T Gershon, Y Gershtein, T Gherghetta, A A Godizov, M C Gonzalez-Garcia, M Goodman, C Grab, A V Gribsan, C Grojean, M Grünewald, A Gurtu, T Gutsche, H E Haber, C Hanhart, S Hashimoto, Y Hayato, A Hebecker, S Heinemeyer, B Heltsley, J J Hernández-Rey, K Hikasa, J Hisano, A Höcker, J Holder, A Holtkamp, J Huston, T Hyodo, K F Johnson, M Kado, M Karliner, U F Katz, M Kenzie, V A Khoze, S R Klein, E Klempt, R V Kowalewski, F Krauss, M Kreps, B Krusche, Y Kwon, O Lahav, J Laiho, L P Lellouch, J Lesgourgues, A R Liddle, Z Ligeti, C Lippmann, T M Liss, L Littenberg, C Lourenço, S B Lugovsky, A Lusiani, Y Makida, F Maltoni, T Mannel, A V Manohar, W J Marciano, A Masoni, J Matthews, U G Meißner, M Mikhasenko, D J Miller, D Milstead, R E Mitchell, K Mönig, P Molaro, F Moortgat, M Moskvic, K Nakamura, M Narain, P Nason, S Navas, M Neubert, P Nevski, Y Nir, K A Olive, C Patrignani, J A Peacock, S T Petcov, V A Petrov, A Pich, A Piepke, A Pomarol, S Profumo, A Quadt, K Rabbertz, J Rademacker, G Raffelt, H Raman, M Ramsey-Musolf, B N Ratcliff, P Richardson, A Ringwald, S Roesler, S Rolli, A Romaniouk, L J Rosenberg, J L Rosner, G Rybka, M Ryskin, R A Ryutin, Y Sakai, G P Salam, S Sarkar, F Sauli, O Schneider, K Scholberg, A J Schwartz, J Schwiening, D Scott, V Sharma, S R Sharpe, T Shutt, M Silari, T Sjöstrand, P Skands, T Skwarnicki, G F Smoot, A Soffer, M S Sozzi, S Spanier, C Spiering, A Stahl, S L Stone, Y Sumino, T Sumiyoshi, M J Syphers, F Takahashi, M Tanabashi, J Tanaka, M Taševský, K Terashi, J Terning, U Thoma, R S Thorne, L Tiator, M Titov, N P Tkachenko, D R Tovey, K Trabelsi, P Urquijo, G Valencia, R Van de Water, N Varelas, G Venanzoni, L Verde, M G Vinciter, P Vogel, W Vogelsang, A Vogt, V Vorobyev, S P Wakely, W Walkowiak, C W Walter, D Wands, M O Wascko, D H Weinberg, E J Weinberg, M White, L R Wiencke, S Willocq, C L Woody, R L Workman, M Yokoyama, R Yoshida, G Zanderighi, G P Zeller, O V Zenin, R Y Zhu, S L Zhu, F Zimmermann, J Anderson, T Basaglia, V S Lugovsky, P Schaffner, and W Zheng. Review of Particle Physics. *Progress of Theoretical and Experimental Physics*, 2020(8):083C01, 08 2020.